Towards comprehension of the surface state properties in the intrinsic magnetic topological insulators

V. N. Men'shov [1,2,3,*] I. A. Shvets,[1,2] and E. V. Chulkov [1,2,4,5,†]

[1]*Tomsk State University, 634050 Tomsk, Russia*

[2]*Saint Petersburg State University, Saint Petersburg 198504, Russia*

[3]*NRC Kurchatov Institute, Kurchatov Sqr. 1, 123182 Moscow, Russia*

[4]*Donostia International Physics Center (DIPC), P. de Manuel Lardizabal 4, 20018 San Sebastián, Basque Country, Spain*

[5]*Departamento de Polímeros y Materiales Avanzados: Física, Química y Tecnología, Facultad de Ciencias Qumicas, Universidad del País Vasco UPV/EHU, 20080 San Sebastián/Donostia, Basque Country, Spain*

(Received 16 August 2022; accepted 24 October 2022; published 3 November 2022)

Presently, the unusual quantum phenomena recently discovered in intrinsic antiferromagnetic topological insulators are far from being fully understood. Motivated by recent controversial ARPES results on the $MnBi_2Te_4$ family compounds, we theoretically study the underlying physics of spectral properties of such materials. By using a continual model, we address the issue of the topological surface fermions which simultaneously experience an exchange field of a regular antiferromagnetic alignment and a surface electrostatic potential. The emergent net exchange field acting on the surface state is shown to depend on the surface potential strength, of which variation could be associated with concentration fluctuations of antisite and other defects that are inevitably present in $MnBi_2Te_4$ material. In this scenario, we discuss the possible microscopic mechanism for change of both size and sign of the surface exchange gap from sample to sample. Furthermore, we provide a natural explanation for the appearance of a finite density of states inside the exchange gap in the case of strong fluctuations in the surface potential. Thus, our results allow for a unified interpretation of various spectroscopic measurements on intrinsic antiferromagnetic topological insulators.

DOI: 10.1103/PhysRevB.106.205301

I. INTRODUCTION

In the past few years, an interplay between topological band structure and magnetic order has become one of the priorities in contemporary condensed matter physics, see, e.g., Ref. [1] and references therein. Such an interplay can give rise to outstanding phenomena including quantum anomalous Hall effect (QAHE) [2] and an axion insulator state [3–5]. In Cr- and/or V-doped films of three-dimensional (3D) topological insulator (TI) $(Bi,Sb)_2Te_3$, the QAHE has taken place at very low temperatures below $T \approx 30$ mK due to nonuniform distribution of dopants and, hence, magnetization [2]. The TI heterostructure engineering, in which magnetic Cr ions are doped into selective quintuple layers (QLs) of the $(Bi,Sb)_2Te_3$ film, has enabled us to elevate the temperature of quantized Hall conductivity up to ∼2 K [6–8]. Besides the magnetic doping, a magnetic proximity effect [9] and a magnetic extension of the TI surface [10] were proposed to achieve an efficient time-reversal symmetry breaking. At the time, Mong *et al.* [11] proposed the existence of 3D TIs with an intrinsic antiferromagnetic (AFM) order. The AFM TI possesses both broken time-reversal Θ and translational $T_{1/2}$ symmetries but preserves the combination $S = \Theta T_{1/2}$ [11]. The recent identification of van der Waals (vdW) compound $MnBi_2Te_4$ [12–15] and its derivatives $MnBi_2Te_4(Bi_2Te_3)_n$ [16,17] as belonging to 3D TIs with out-of-plane AFM order of the A type has sparked off a fresh wave of explorations in the quantum materials area. In $MnBi_2Te_4$ flakes with an odd number of septuple layers (SLs), a spontaneous (i.e., under zero external magnetic field) QAHE was observed at $T = 1.4$ K, and a robust transverse conductivity plateau of $\cong e^2/h$ was obtained at $T = 6.5$ K upon increasing perpendicular external magnetic field up to moderate value 7.6 Tesla [14]. In $MnBi_2Te_4$ samples with an even number of SLs, a magnetic-field-driven topological phase transition between an axion insulator state and QAHE was found [15]. Ge *et al.* reported the experimental observation in $MnBi_2Te_4$ eight-SL films of a nearly quantized Hall resistance plateau (without Landau levels) surviving above the Néel temperature up to 45 K [18]. The underlying microscopic mechanisms behind the unconventional properties of the $MnBi_2Te_4$ family materials are still not well understood and remain a debated subject [19,20].

The topologically protected surface states are the ones responsible for providing quantum transport in magnetic 3D TIs [21–25]. The spectral properties of the surface states in the $MnBi_2Te_4$ family, despite the significant experimental and theoretical advances, are still a debated matter. In theory, the combined S symmetry is broken at the ferromagnetic (FM) surface of AFM TI, therefore an exchange gap arises in the Dirac-cone-like dispersion of the surface state [11]. The first-principles calculations for the ideal (0001) surface of the AFM TI $MnBi_2Te_4$ predict the sizable gap, which may attain to 88 meV [12,26,27]. Indeed, a number of angle-resolved photoemission spectroscopy (ARPES) studies of the $MnBi_2Te_4$ single crystals below the Néel temperature $T_N \approx 24$ K confirmed the predicted gap opening in the Dirac

*vnmenshov@mail.ru

†evguenivladimirovich.tchoulkov@ehu.es

 ©2022 American Physical Society

electron spectrum at the (0001) surface, estimated at tens of meVs [12,28–31]. The photoemission measurements, conducted out for different $MnBi_2Te_4$ samples grown by two chemist groups showed that the gap size is ranging from relatively small ∼15 meV to large size ∼65 meV [32]. Remarkably, using the laser-ARPES technique, Shikin *et al.* observed both a large energy gap ∼60 meV and a reduced one $\lesssim$20 meV for distinct areas within the same (0001) surface [33]. However, some other groups after having carried out the high-resolution ARPES investigations have arrived at an alternative conclusion related to the behavior of the surface states in $MnBi_2Te_4$ featuring a gapless character [34–39].

According to Refs. [34,36,37,40,41], the reason for the vanishing gap in the ARPES surface spectrum of AFM TI $MnBi_2Te_4$ lies in a reorientation of the surface Mn magnetic moments from the out-of-plane direction to the basic plane or a strong suppression of the magnetic ordering in the uppermost SL. However, having conducted static and time-resolved ARPES with full polarization control of $MnBi_2Te_4$, Nevola *et al.* [38] reached the conclusion that the magnetic order is retained at the (0001) surface. The magnetic force microscopy study [42] also provided evidence that the robust uniaxial A-type order persists to the top surface layers in $MnBi_2Te_4$. The data obtained from x-ray magnetic circular dichroism measurements [12,33] do not point to the magnetization change at the $MnBi_2Te_4$ surface either. Thus, the assumptions on the possible surface magnetization relaxation [34,36] are inconsistent with the experimental facts for the prototypical intrinsic AFM TI [12,33,38,42].

In searching for the nature of the driving force for the gap modulation in the surface state spectrum in $MnBi_2Te_4$, attention has been drawn to the factors which are not directly linked solely to the magnetic order. For example, the scanning tunneling microscopy and x-ray diffraction experiments [30,43,44] showed that native antisite cation defects Bi_{Mn} (Bi at Mn site) and Mn_{Bi} (Mn at the Bi site) as well as Bi_{Te} antisites (Bi atoms at the Te sites) and Te vacancies in enough high concentrations are always presented in the $MnBi_2Te_4$ crystal samples. The redistribution of the charge density near the (0001) surface caused by random spatial fluctuations of the antisite defects in $MnBi_2Te_4$ results in local density of states near the Fermi level, as observed by scanning tunneling spectroscopy [43]. The scanning tunneling microscopy and spectroscopy revealed that $MnBi_2Te_4$ usually contains a few percent of Mn_{Bi} and Bi_{Mn} antisite defects, while the average density of Bi_{Te} defects is several tenths of a percent [30,43–45], although Ref. [46] exhibits that, in thin film $MnBi_2Te_4$, the defective areas with high local concentrations of Mn_{Bi} (∼9%) are adjacent to defect-free areas. It should also be borne in mind that the as-grown bulk $MnBi_2Te_4$ samples are usually heavily degenerate *n*-type semiconductors, with the Fermi level located inside the conduction band [12,34,36,43,47]. The Bi_{Mn} antisite is the most common *n*-type dopant [48].

Apart from the point defects, the $MnBi_2Te_4$ surface can contain other structural imperfections such as unavoidable steps, deformations, or relaxations. Moreover, the scanning transmission electron microscopy in few-SL exfoliated $MnBi_2Te_4$ samples [49] observed a surface disintegration, where the topmost SL stratifies into a Mn-doped Bi_2Te_3 QL and a Mn_xBi_yTe double layer.

The density functional theory (DFT) studies of the surface spectra of AFM TIs recently done in Refs. [32,33,44] took into account a deviation of the $MnBi_2Te_4$ crystal structure from the ideal one that is brought on by the presence of the above-mentioned intrinsic defects. As these DFT calculations demonstrate, the gap size of the topological surface states is determined by the redistribution of the electron density near the (0001) surface, albeit the source and character of the redistribution may be different. In Ref. [33], the Mn-Bi antisite defects and mechanical cleavage distortions are suggested to tend to cause interblock vdW spacing expansion, which is accompanied by a relocation of the surface state toward the second SL block; as a consequence, the gap is reduced proportionally to the net exchange field (NEF) felt by the surface electron. The authors of Ref. [32] introduced in their DFT calculations an uncompensated surface charge, which can reflect the presence of the Mn-Bi antisite defects in the surface region. They described the structure of the surface state in both real and momentum space as a function of magnitude and sign of the surface charge. The simulations [44] showed the gap can be strongly reduced because the probability density of the topological surface state is predominantly localized near the Bi layers that contain the Mn_{Bi} magnetic moments oppositely directed with respect to the Mn layer moments.

In this paper, we propose an analytical approach that provides an explanation for the ambiguous behavior of the topological surface states in intrinsic AFM TIs like the prototypical compound $MnBi_2Te_4$. We use a rather simple model based on the incorporation of an effective surface potential (ESP), which is a driving force for the surface electron structure modification. Our scenario makes it possible to reproduce both gapped and gapless surface spectra depending on the ESP character under the assumption that the AFM order is persistent near the surface. Moreover, our theoretical formalism highlights the role of electrostatic inhomogeneity, which can be linked to random spatial distribution of the anti-site defects among the Mn and Bi sub-lattices and other defects, in understanding the gapless surface states of the intrinsic AFM TIs.

The rest of the paper is organized as follows. In Sec. II, we formulate the conceptional idea and design a theoretical model for the surface states of AFM TI, which are driven by ESP. In Sec. III, we show analytically how the size and sign of the exchange gap in the surface fermions dispersion are determined by the spatially uniform ESP strength. Section IV is dedicated to an estimation of the surface density of states under a weak electrostatic disorder. Section V deals with the bound in-gap states occurring at domain walls of exchange fields that are generated by inhomogeneous ESP. In Sec. VI, we analyze the averaged spectral properties inherent to the AFM TI surface subjected to strong electrostatic disorder. Finally, in Sec. VII, we discuss our results in light of the ARPES experimental data and draw conclusions.

II. CONTINUAL MODEL OF THE TOPOLOGICAL SURFACE STATES IN INTRINSIC AFM TI

The ternary compounds of the $MnBi_2Te_4$ family with general chemical formula MPn_2Ch_4, where Pn = (Sb, Bi) and Ch = (Se, Te), crystallize in a tetradymite-type crystal

structure built of the SL blocks stacked along the $\mathbf{e}_z$ direction and linked to each other through the weak vdW forces. Every such SL block can be viewed as a sequence of covalently bonded atomic layers $Ch_1 - Pn_1 - Ch_2 - M - Ch_3 - Pn_2 - Ch_4$, in which a central layer consists of *3d* transition-metal atoms M = (Mn, V, Cr). The topological electron properties of MPn_2Ch_4 are mainly dominated by four states around the Fermi level: the bonding states composed of the p_z orbitals of atoms in the cation layers Pn_1 and Pn_2, $|Pn+\uparrow(\downarrow)\rangle$, and the antibonding states composed of the p_z orbitals of atoms in the chalcogen layers Ch_1 and Ch_4, $|Ch-\uparrow(\downarrow)\rangle$, where indices $+/-$ and $\uparrow/\downarrow$ denote the parity and spin projection onto the quantization axis $\boldsymbol{e}_z$, respectively [27]. These low-energy states form the minimal basis $u_\Gamma = \{|Pn+\uparrow\rangle, |Ch-\uparrow\rangle, |Pn+\downarrow\rangle, |Ch-\downarrow\rangle\}$ suitable for the construction of the 3D $\mathbf{k}\cdot\mathbf{p}$ Hamiltonian of the system near the Γ point of the Brillouin zone as an expansion in the powers of the momentum $\mathbf{k} = (k_x, k_y, k_z)$:

$$H_T(\mathbf{k}) = (\Xi - \mathrm{B}k^2)\tau_z \otimes \sigma_0 + \mathrm{A}\tau_x \otimes (\boldsymbol{\sigma}\cdot\mathbf{k}). \quad (1)$$

Here 2Ξ is an energy band gap at $\mathbf{k} = 0$, B describes a band curvature, A is a matrix element of the velocity operator, σ_α and τ_β ($\alpha, \beta = 0, x, y, z$) denote the Pauli matrices in the spin and orbital space, respectively, and $k = |\mathbf{k}|$. To simplify the analysis, the Hamiltonian Eq. (1) is assumed to be is isotropic in $\mathbf{k}$ and particle-hole symmetric. The condition $\Xi\mathrm{B} > 0$ reflects the inverted order in energy of the basis states around $\mathbf{k} = 0$ due to strong spin-orbit coupling, as in the $MnBi_2Te_4$ bulk. Note that $H_T(\mathbf{k})$ Eq. (1) is a conventional $\mathbf{k}\cdot\mathbf{p}$ Hamiltonian of a nonmagnetic 3D TI [27].

The 3*d* states of the M atoms are usually far away from the energy of p_z states and have a large exchange splitting of the order of a few eV [26]. The magnetic moments localized at these atoms are expected to align in parallel within single SL block thanks to the *M-Ch-M* superexchange interaction mediated by chalcogen ions in adjacent layers Ch_2 and Ch_3 [27]. The interaction between the magnetic moments of neighboring SLs being transmitted via the long atomic chain crossing a vdW interval, $M - Ch_3 - Pn_2 - Ch_4||Ch_1 - Pn_1 - Ch_2 - M$, is relatively weak. The above exchange interactions may lead to the appearance of the long-rang magnetic order. For example, in the bulk $MnBi_2Te_4$ below 25 K, there exists an AFM phase of the A type with easy axis pointing along the $\mathbf{e}_z$ direction.

Taking into account that the topological band states are mainly formed by the orbitals of atoms in the layers Ch_1, Pn_1, Pn_2, Ch_4, while the orbitals of atoms in the layers Ch_2, M, Ch_3 are responsible for the magnetic ordering, the system can be viewed as a periodic AFM texture embedded into a 3D TI host. Therefore, the bulk Hamiltonian for a AFM TI can be given just by adding perturbative exchange term H_{ex} to Eq. (1), which can be written down in the basis u_Γ as $H_{\mathrm{ex}}(z) = \mathrm{diag}\{J_1, J_2, -J_1, -J_2\}mf(z)$. In the following discussion, we restrict ourselves to the case when the 3*d*-atom moments are perpendicular to the layer plane, $\mathbf{m} = \mathbf{e}_z m$. The effective exchange integrals J_1 and J_2 are related to the states $|Pn+\uparrow(\downarrow)\rangle$ and $|Ch-\uparrow(\downarrow)\rangle$, respectively; generally speaking, $J_1 \neq J_2$. The off-diagonal matrix elements in H_{ex} are negligibly small. In the ground state, the alternation of the magnetization distribution $mf(z)$ along the out-of-plane axis can be described by the periodic function $f(z) = f^{(A)}(z) = f^{(A)}(z + 2cn)$ ($n = 0, \pm1, \pm2, \ldots$) and $f^{(A)}(z \pm c) = -f^{(A)}(z)$. In addition, we put the condition $\frac{1}{c}|\int_{\langle \mathrm{SL}\rangle} f(z)dz| = 1$, where the integration is performed over the SL block height c. The magnetic texture of the $MnBi_2Te_4$-like material is sensitive to an external field $\mathbf{H}$. So, under relatively weak field $\mathbf{H}\|\mathbf{e}_z$, applied normal to the basal plane, it undergoes the spin-flop transition to a fully polarized FM phase [12,45,50], then one takes $f(z) = f^{(F)}(z)$ with $f^{(F)}(z) = f^{(F)}(z + cn)$ ($n = 0, \pm1, \pm2, \ldots$).

The surface properties of the intrinsic AFM TI are in the focus of our paper. An electron density redistribution arises near the boundary of a perfect semiconductor. In the real compound $MnBi_2Te_4$, a spatially inhomogeneous electron density is an unavoidable consequence of concentration fluctuations of charged defects such as the antisites Bi_{Mn} and Mn_{Bi} in a sample [30,43,44]. A similar situation might also be the case for other compounds MPn_2Ch_4. As a result of cleavage, the regions of uncompensated positive and/or negative charge can occur at the emergent (0001) surface due to the Mn-Bi intermixing (as well as the Te vacancies and other defects), whereas the sample remains electrically neutral on average. The long-range Coulomb interaction is implied to be included in the consideration, thereat note that the screening effects are different in the bulk and at the surface. The mentioned factors result in perturbation of topmost layers of the truncated crystal, thereby providing input into the random potential $V_S(\mathbf{r})$ affecting the electronic structure at the AFM TI surface. The electrostatic modification of the near-surface region can phenomenologically be incorporated into the model via the term $H_S = V_S - V_B$, which is defined as the difference between the surface potential V_S and the bulk potential V_B expressed in the basis u_Γ [51]. Thereafter, we refer to H_S as an ESP. We consider a semi-infinite slab of 3D material, such as $MnBi_2Te_4$ (MPn_2Ch_4), occupying the region $z > 0$. The material boundary located at $z = 0$ is suggested to be perfectly flat and coincident with the (0001) surface terminated by the layer Ch_1. All in all, the full electron energy functional of the semi-infinite 3D AFM TI reads

$$\Omega = \int_{z\geqslant 0} d\mathbf{r}\Theta^+(\mathbf{r})[H_T(-i\Delta) + H_{\mathrm{ex}}(z) + H_S(\mathbf{r})]\Theta(\mathbf{r}), \quad (2)$$

where $\Theta(\mathbf{r})$ is the spinor envelope function (EF), $\Theta = (\theta_1^\uparrow, \theta_2^\uparrow, \theta_1^\downarrow, \theta_2^\downarrow)^t$, the superscript t denotes the transpose operation, $\mathbf{r} = (x, y, z)$.

We assume that ESP is confined near the surface at short length $\sim d$. As long as the EF spatial variation in the direction $\mathbf{e}_z$ is sufficiently slow on the scale d, one can adopt a local approximation, $H_S(\mathbf{r}) = U(x, y)d\delta(z)$, for an analytic calculation. Furthermore, we consider the antisite defects as a major contributor to ESP and the contribution is of an electrostatic nature. Therefore, the ESP matrix can be expressed in the diagonal form: $U = \mathrm{diag}\{U_1, U_2, U_1, U_2\}$. The components $U_{1,2}(x, y)$ describe the EPS long-range lateral landscape related to the concentration fluctuations of the antisite defects along the surface plane (x, y) at the distances much longer that the atomic spacing.

III. HOMOGENEOUS ESP APPROXIMATION

The functional Eq. (2) determined about the Γ point allows describing the low-energy long-wavelength properties of the system near the surface. We begin by considering the effect of the homogeneous ESP, when $U(x, y) = \text{const}$, on the surface state of intrinsic AFM TI. In this case, the surface displays translation symmetry, hence, the in-plane momentum $\boldsymbol{\kappa} = (k_x, k_y)$ is a good quantum number. The variational procedure for the energy functional (2) leads to the equations for EF in the half-space $z > 0$:

$$[H_T(\boldsymbol{\kappa}, -i\partial_z) + H_{ex}(z) - IE]\Theta(\boldsymbol{\kappa}, z) = 0, \tag{3}$$

$$\left[\frac{\delta H_T(\boldsymbol{\kappa}, -i\partial_z)}{\delta(-i\partial_z)} - 2dU\right]\Theta(\boldsymbol{\kappa}, z)|_{z=0} = 0, \tag{4}$$

where $\partial_z = \partial/\partial z$, I is a unit 4×4 matrix. We look for the eigenstate of the boundary problem (3)-(4), for which EF vanishes apart from the surface, $\Theta(\kappa, z \to \infty) = 0$, and the eigenvalue lies within the bulk gap, $|E(\boldsymbol{\kappa})| < \Xi$. The surface perturbation H_S does not affect the inverted bulk gap that guaranties the surface state existence, however, the characteristics of a such state can be significantly altered with the varying boundary conditions. In our approach, the *natural* boundary conditions Eq. (4), imposed on the EF at the surface, contain ESP U [23,51,52]. Note that the application of the *open* boundary condition with EF vanishing at the surface cannot provide a simulation of either the electrostatic surface effect or the magnetic proximity effect at an interface [25].

To solve the problem, we resort to the formalism [24,53] that allows us to reduce the 3D model of the semi-infinite AFM TI (2) to a two-dimensional (2D) effective Hamiltonian $H_{2D}(\boldsymbol{\kappa})$. To this end, we in fact perform the perturbation procedure in the small parameters $(|\frac{J_{1,2}m}{\Xi}|, |\frac{A\kappa}{\Xi}|, \frac{B\kappa^2}{\Xi}) \ll 1$. In zeroth approximation (at $\boldsymbol{\kappa} = 0$ and $H_{ex} = 0$), Eqs. (3) and (4) may be solved exactly. Although we can determine the ESP matrix in the most general case, without loss of generality, we focus our discussion on a particular case $U_1 = -U_2 = U$, when the solution acquires remarkably simple form. The straightforward calculations lead to the eigenvalue $E_0 = 0$ and the spinor EF $\Theta_0(z) = (1, i, 1, -i)^t\theta_0(z)$, where

$$\theta_0(z) = D[\exp(-q_1 z) + \gamma\exp(-q_2 z)], \tag{5}$$

D is a normalization constant satisfying the condition $2\int_0^\infty dz\ \theta^2(z) = 1$, $\gamma = \frac{\sqrt{\lambda-1}-\widetilde{U}}{\sqrt{\lambda-1}+\widetilde{U}}$, $\widetilde{U} = dq_0\frac{U}{\Xi}$, hereafter the superscript $\sim$ indicates dimensionless variables. It should be noted that the penetration lengths of the topological surface state Eq. (5) $\sim q_{1,2}^{-1}$ are determined only by the parameters of the 3D Hamiltonian Eq. (1): $q_{1,2} = q_0[\sqrt{\lambda} \pm \sqrt{\lambda-1}]$, $q_0 = \sqrt{\frac{\Xi}{B}}$, $\lambda = \frac{A^2}{4B\Xi}$. Throughout the paper, for the sake of certainty, the case $\lambda > 1$ is adopted. Equation (5) describes the effect of ESP of arbitrary strength U on the EF spatial behavior. Indeed, with increasing ESP strength, the EF profile Eq. (5) evolves gradually from the sum of the exponents at $U = 0$ to the difference between the exponents as $|\widetilde{U}| \gg 1$. Correspondingly, while at the weak ESP, $|\widetilde{U}| \leqslant 1$, EF is mostly localized near the surface, it shifts toward the bulk as the strength $|\widetilde{U}|$ grows. In the case of the strong ESP, $|\widetilde{U}| \gg 1$, the gravity center of the state is placed at the distance $c \sim q_0^{-1}$ from the surface. To clearly demonstrate these trends, we depict in Fig. 1 the profile of the square of normalized EF of the surface state for several values $\widetilde{U}$.

One can construct the orthonormal basis from two spinors $\Phi^\uparrow(z) = (1, i, 0, 0)^t\theta_0(z)$ and $\Phi^\downarrow(z) = (0, 0, 1, -i)^t\theta_0(z)$; indeed $\langle\Phi^\uparrow|\Phi^\uparrow\rangle = \langle\Phi^\downarrow|\Phi^\downarrow\rangle = 1$ and $\langle\Phi^\uparrow|\Phi^\downarrow\rangle = 0$. Within the frame of this basis, we derive the 2D effective Hamiltonian:

$$H_{2D}(\boldsymbol{\kappa}) = A(k_x\sigma_y - k_y\sigma_x) + \Delta\sigma_z, \tag{6}$$

$$\Delta = \frac{J_1 + J_2}{2}mQ = \Delta_0 Q, \tag{7}$$

$$Q = 2\int_0^\infty dz\ \theta_0^2(z)f(z). \tag{8}$$

The lack of terms quadratic in momentum $\boldsymbol{\kappa}$ in Eq. (6) is attributable to the condition $U_1 = -U_2$, under which the particle-hole symmetry remains. Equations (6)–(8) demonstrate that the spin degree of freedom of the surface fermion experiences the NEF Δ. The latter represents a direct measure of the uncompensated magnetization gathered over the near-surface region of AFM TI in accordance with the distribution $f(z)$ and proportional to the probability electron density therein $\sim\theta_0^2(z)$ Eq. (5). The spectrum of the Hamiltonian Eq. (6) has a form of the gapped 2D Dirac cone $E(\boldsymbol{\kappa}) = \pm\sqrt{A^2\kappa^2 + \Delta^2}$. Hence, we analytically find that the exchange gapping of the surface state being proportional to NEF is sensitive to the variation of ESP. It is an important result of the paper.

Let us consider how the mechanism of the modification of the surface electron structure works on the simple example, where EF $\theta_0(z)$ is given by Eq. (5), whereas the magnetization distribution $f(z)$ in the semi-infinite AFM TI is presented as

$$f^{(A)}(z) = c\sum_{n=0}^{\infty}(-1)^n\delta\left[z - \left(n + \frac{1}{2}\right)c\right] \tag{9}$$

for the A-type AFM order in the ground state and

$$f^{(F)}(z) = c\sum_{n=0}^{\infty}\delta\left[z - \left(n + \frac{1}{2}\right)c\right] \tag{10}$$

for the metastable FM order realized under external magnetic field, where $\delta(z)$ is the delta function. The magnetization in Eqs. (9) and (10) is assumed to be concentrated in the middle of each structural SL block. Correspondingly, we obtain the explicit relations

$$Q^{(A)} = cD^2\left[\frac{1}{\cosh(q_1 c)} + \frac{2\gamma}{\cosh\left(\frac{q_1+q_2}{2}c\right)} + \frac{\gamma^2}{\cosh(q_2 c)}\right], \tag{11}$$

$$Q^{(F)} = cD^2\left[\frac{1}{\sinh(q_1 c)} + \frac{2\gamma}{\sinh\left(\frac{q_1+q_2}{2}c\right)} + \frac{\gamma^2}{\sinh(q_2 c)}\right], \tag{12}$$

where $D^2 = [\frac{1}{q_1} + \frac{4\gamma}{q_1+q_2} + \frac{\gamma^2}{q_2}]^{-1}$. Thus, the integral dependence of the Q factor Eq. (8) on the product $\theta_0^2(z)f(z)$ is parameterized by means of the ESP strength U and the crystal lattice period c. It is convenient to compare the period c with the length at which the surface state penetrates into the bulk; therefore, we use below the dimensionless period $\widetilde{c} = cq_0$.

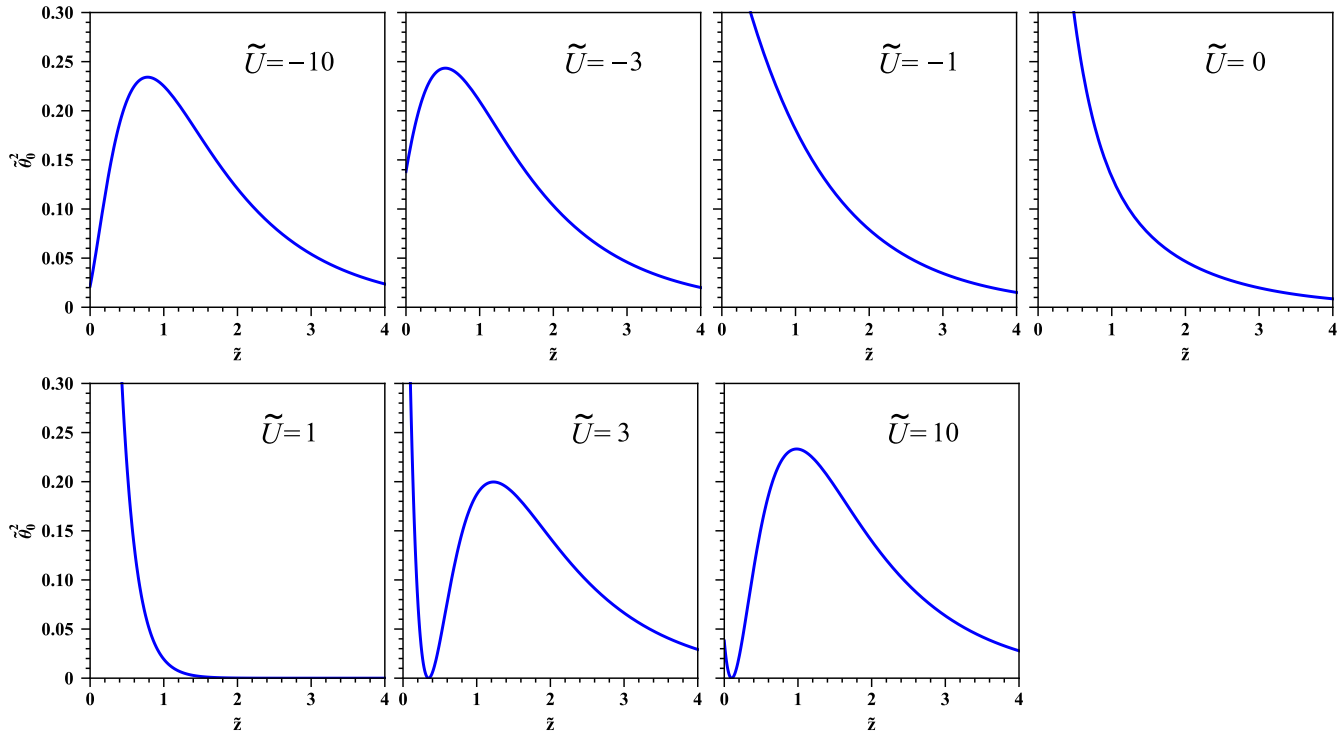

FIG. 1. Evolution of the spatial profile of the envelope function square Eq. (5) versus the effective surface potential strength, $\widetilde{z} = zq_0$. The band structure parameter is $\lambda = 2$.

In the case of the A-type AFM order, the Q factor as a function of $\widetilde{c}$ decays exponentially at $\widetilde{c} \gg 1$ and vanishes as $\widetilde{c} \to 0$. The dependence $Q^{(A)}(\widetilde{U}, \widetilde{c})$ has a complicated character in the region of relatively small and intermediate period c, i.e., $\widetilde{c} \lesssim 1$. This is the most relevant in the context of our consideration because the surface state can be extended to the second-third SL [32,33,44]. In Fig. 2, the Q factor $Q^{(A)}(\widetilde{U}, \widetilde{c})$ is plotted as a function of the strength $\widetilde{U}$ at the different periods $\widetilde{c}$ for fixed value of the parameter λ. The Q factor is saturated at the large strength $|\widetilde{U}|$. The saturation level $Q^{(A)}(|\widetilde{U}| \to \infty) = Q_{\infty}^{(A)}$ depends on $\widetilde{c}$ and λ (see Fig. 3) and attains a maximum at $\widetilde{c} \gtrsim 3$. However, the Q factor $Q_{\infty}^{(A)}$ is negative in the region $0 < \widetilde{c} < \widetilde{c}_0$, where the parameter $\widetilde{c}_0$ satisfies the equation $\sinh^2(\widetilde{c}\sqrt{\lambda}) = \cosh(\widetilde{c}\sqrt{\lambda - 1})$. In turn, Fig. 2 provides the small-scale picture for $Q^{(A)}(\widetilde{U}, \widetilde{c})$ with much higher resolution at small or moderate values of $|\widetilde{U}|$. As can be seen in Fig. 2, when $\widetilde{c} > \widetilde{c}_0$, the Q factor is reduced considerably compared to the saturation level $Q_{\infty}^{(A)}$ near $\widetilde{U} \gtrsim 1$ and can even make it negative. In contrast, when $\widetilde{c} < \widetilde{c}_0$, the Q factor reaches a peak about $\widetilde{U} \sim 1$.

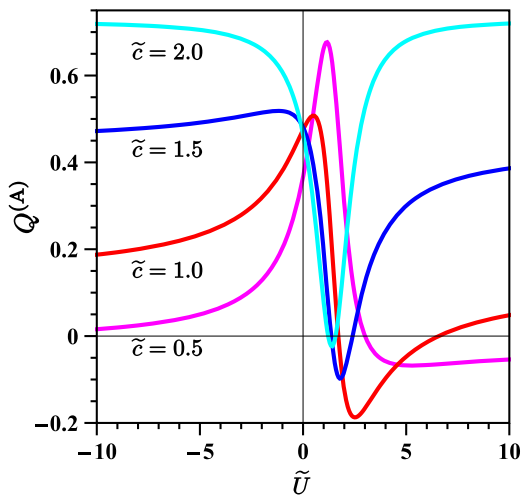

FIG. 2. The image of the Q factor $Q^{(A)}(\widetilde{U}, \widetilde{c})$ is plotted as a function of the ESP strength $\widetilde{U}$ for different periods $\widetilde{c}$ (= 0.5; 1.0; 1.5; 2.0) and fixed value of the parameter $\lambda = 2$.

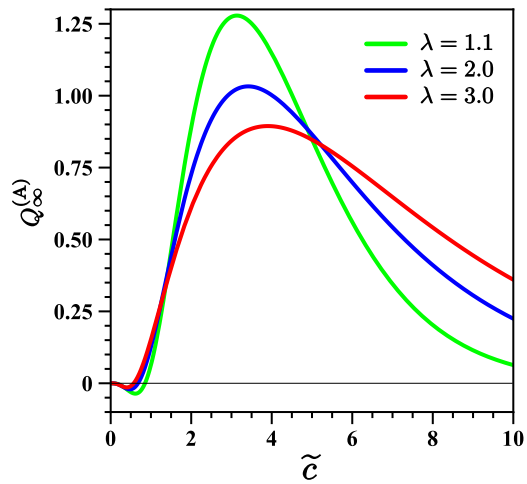

FIG. 3. The dependence of the saturation level of the Q factor $Q_{\infty}^{(A)}$ on period $\widetilde{c}$ at different values λ (= 1.1; 2.0; 3.0).

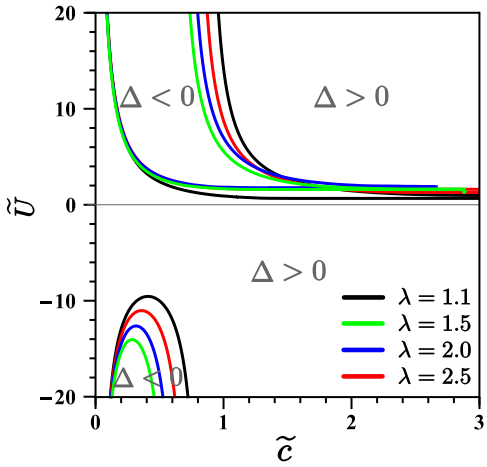

FIG. 4. The topological diagram for the AFM TI surface in the terms of the closing and reopening of the exchange gap in the surface spectrum on the parametric plane $(\widetilde{U}, \widetilde{c})$. The regions with the positive and negative gaps are separated from each other by the lines $\widetilde{U}_{\pm}(\widetilde{c})$ depicted in color at different values of the parameters $\lambda = 1.1$ (black), 1.5 (red), 2.0 (blue), 2.5 (green).

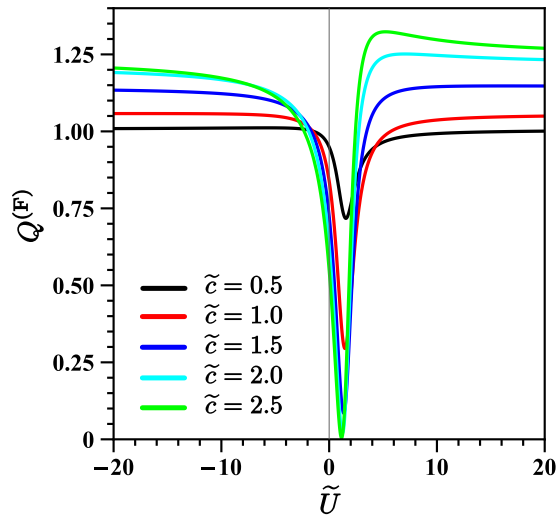

FIG. 5. The large-scale image of the Q factor $Q^{(F)}(\widetilde{U}, \widetilde{c})$ is plotted as a function of the ESP strength $\widetilde{U}$ at the different periods $\widetilde{c}$ $(= 0.5; 1.0; 1.5; 2.0; 2.5)$ for fixed values of the parameter $\lambda = 2$.

Under changing strength of SP, the Q factor $Q^{(A)}(\widetilde{U}, \widetilde{c})$ and, as a consequence, the exchange gap in the surface state spectrum $\Delta^{(A)}(\widetilde{U}, \widetilde{c}) = \Delta_0 Q^{(A)}(\widetilde{U}, \widetilde{c})$ not only vary in the size in a wide range but also invert the sign. Figure 4 presents the model diagram in the space of the parameters $(\widetilde{U}, \widetilde{c})$, which depicts the sectors of the positive and negative $\Delta^{(A)}(\widetilde{U}, \widetilde{c})$. These sectors are delimited from each other by the continuous lines $\widetilde{U}_{\pm}(\widetilde{c})$, where $\widetilde{U}_{\pm}(\widetilde{c})$ are two real roots of the equation $Q^{(A)}(\widetilde{U}, \widetilde{c}) = 0$. The transition across the line $\widetilde{U}_{\pm}(\widetilde{c})$ is accompanied by the closing and reopening of the exchange gap. When $\widetilde{c} < \widetilde{c}_0$, the sector with the positive gap falls within the interval $\widetilde{U}_+ > \widetilde{U} > \widetilde{U}_-$. Correspondingly, at $\widetilde{U} > \widetilde{U}_+$ or $\widetilde{U} < \widetilde{U}_-$, the gap is of the negative sign, when the NEF is aligned antiparallel to the magnetization of the upmost SL. In particular, if $|\widetilde{U}| \gg 1$, the location of two regions with the negative gap on the plane $(\widetilde{U}, \widetilde{c})$ is described by the inequalities $\frac{2}{|\widetilde{U}|} < \widetilde{c} < \widetilde{c}_0 + \frac{\beta(\lambda)}{\widetilde{U}}$, where $\beta\lambda$ is a positive quantity of the order of unity, an explicit form of which is omitted here owing to the cumbersomeness. On the other hand, when $\widetilde{c} \gg 1$, the region with $\Delta^{(A)}(\widetilde{U}, \widetilde{c}) < 0$ is confined within the interval $\widetilde{U}_+ > \widetilde{U} > \widetilde{U}_-$, where $\widetilde{U}_{\pm}(\widetilde{c}) = \sqrt{\lambda - 1}[1 + 2\exp(-\widetilde{c}\sqrt{\lambda - 1}) \pm 2\exp(-\widetilde{c}\sqrt{\lambda})]$.

The main physical reason of a such nontrivial behavior NEF felt by the surface state goes back to the variation of the EF square profile $\theta_0^2(z)$, Eq. (5), versus the ESP strength. The ESP tends to push the surface state inward the bulk on the distance $z = z_{\max}$. Provided that ESP is sufficiently weak, the surface state is mostly placed close to the surface, i.e., within the outermost SL at $\frac{1}{2}c \approx z_{\max}$, therefore NEF is positive, $\Delta^{(A)} > 0$. However, at $|\widetilde{U}| \gg 1$, the gravity center of the density $\theta_0^2(z)$ is remarkably displaced away off the surface, as seen in Fig. 1. If one assumes that $\frac{3}{2}c \approx z_{\max}$, NEF is certainly contributed by the second SL, the magnetization of which is opposite to that of the first SL, hence NEF is negative, $\Delta^{(A)} < 0$. Indeed, by comparing the dependence $z_{\max}(\lambda, |\widetilde{U}| \to \infty) = \frac{\ln(\sqrt{\lambda}+\sqrt{\lambda-1})}{q_0\sqrt{\lambda-1}}$ with that $c_0(\lambda)$, it is clear that the location of the gravity center of $\theta_0^2(z)$ in the middle of the second SL corresponds to a deep interior of the regions with $\Delta^{(A)} < 0$ on the diagram in Fig. 4, roughly speaking, about $c \approx \frac{1}{2}c_0$. When the ESP strength has a moderate value and positive sign, $\widetilde{U} > \sqrt{\lambda - 1}$, the EF becomes zero, $\theta_0(z_0) = 0$, at $z_0 = \frac{\ln|\gamma|}{2q_0\sqrt{\lambda-1}}$ (Fig. 1). One can choose the ESP strength in such a way that the probability density $\theta_0^2(z)$ decays near $\frac{1}{2}c$ (i.e., $\frac{1}{2}c \approx z_{\min}$), then the contribution from the first SL is almost reduced, and NEF may be negative even if $\widetilde{c} \gg \widetilde{c}_0$. Otherwise, for large c, the sign of NEF $\Delta^{(A)}$ coincides with the magnetization sign in the first SL. Thus, the reversal in the surface exchange gap sign under ESP is a very important feature of the intrinsic AFM TI in the ground state.

In the case of the FM inter-SL alignment, the NEF expectation value $\Delta^{(F)}(\widetilde{U}, \widetilde{c}) = \Delta_0 Q^{(F)}(\widetilde{U}, \widetilde{c})$ is always positive. Shown in Fig. 5 is the Q factor $Q^{(F)}(\widetilde{U}, \widetilde{c})$ as a function of the strength $\widetilde{U}$ at the different periods $\widetilde{c}$ for a fixed value of the parameter λ. One sees that the Q-factor is saturated at the large ESP strength $|\widetilde{U}| \gg 1$ and declines in the vicinity $\widetilde{U} \approx \sqrt{\lambda - 1}$ compared to the saturation level $Q_\infty^{(F)}$. The saturation level $Q_\infty^{(F)} = Q^{(F)}(|\widetilde{U}| \to \infty)$ depends on $\widetilde{c}$ and λ. It attains a maximum at $\widetilde{c} \approx 2.5$ and decays drastically at $\widetilde{c} \gg 1$. The overall behavior of $Q^{(F)}(\widetilde{U}, \widetilde{c})$ seems to be similar to that of $Q^{(A)}(\widetilde{U}, \widetilde{c})$; furthermore, at $\widetilde{c} > 1$ the difference between the NEF expectation values $\Delta^{(F)}(\widetilde{U}, \widetilde{c})$ and $\Delta^{(A)}(\widetilde{U}, \widetilde{c})$ do not exceed 10–15%, though at small $\widetilde{c}$ they display very distinct trends: the level $Q_\infty^{(A)}$ decreases drastically and even changes its sign at $\widetilde{c} \leqslant 1$ (Fig. 3), while the level $Q_\infty^{(F)}$ approaches unit if $\widetilde{c} \to 0$ (Fig. 5).

IV. SURFACE DENSITY OF STATES UNDER A WEAK ESP DISORDER

Electrostatic perturbation of the surface states, being caused by random distribution of the charged antisite and other defects on the intrinsic AFM TI surface, can

significantly changes from one sample to another and is even able to vary appreciably along the same sample surface. Having described in the previous section the mechanism underlying the exchange gap modulation under the assumption that ESP is uniform along the surface plane (x, y), raises a question about how fluctuations in the ESP strength drive spectral properties of the topological surface states. In macroscopic measurements, the observable characteristics are normally averaged over the sample in convoluted way. For the moment, we restrict ourselves to an analysis of the surface density of states (DOS). To this end, assuming a weak disorder of the antisite defects, we estimate the dependence of DOS on ESP under relatively small fluctuations of the strength U.

Within our model, in the situation of an high-quality samples associated with the uniform ESP strength U along the whole surface, the emergent NEF opens the gap in the dispersion law $E(\boldsymbol{\kappa}) = \pm\sqrt{\mathrm{A}^2\kappa^2 + \Delta^2}$, thus leading to 2D DOS

$$N_{2\mathrm{D}}(E|U) = \frac{a^2|E|}{2\pi\,\mathrm{A}^2} h(|E| - |\Delta(U)|), \tag{13}$$

where the gap size $2\Delta(U)$ follows the strength U in accordance with Eqs. (7), (8), (11), and (12), a is the surface lattice constant, $h(E)$ is the Heaviside function. Therefore, in the case of weakly fluctuating ESP, the averaged DOS is composed of different partial $N_{2\mathrm{D}}(E|U)$ Eq. (13) accordingly to their statistic weight $P(U)$, i.e. $\langle N_{2\mathrm{D}}(E)\rangle = \int dU P(U) N_{2\mathrm{D}}(E|U)$. In such simple manner of averaging, one can estimate a fluctuation-induced smearing of the band-edges. To this end, we define the strength fluctuation distribution via the Gaussian function $P(U) = \frac{1}{\sqrt{2\pi}W}\exp[-\frac{(U-U_0)^2}{2W^2}]$ assuming that mean-squared fluctuations $\sim W$ are small as compared with the characteristic scale of U in which the Q-factor varies profoundly, in other words, $W \ll |U_\pm|$. In this case, the behavior of $\langle N_{2\mathrm{D}}(E)\rangle$ is directly related to the location of the mean strength U_0.

Of primary interest for us is the parameter region $\widetilde{c} < \widetilde{c}_0$, where the typical dependence $Q^{(A)}(\widetilde{U}, \widetilde{c})$ is exemplified by the curve at $\widetilde{c} = 0.5$ in Figs. 2(a) and 2(b). For the large strength $|U_0|$, the Q factor changes weakly. In such a case, the averaged DOS is expressed by the form of Eq. (13) in which $\Delta = \Delta_0 Q^{(A)}_\infty$. On the other hand, in the region of the moderate values of ESP, $U_- < U_0 < U_+$, the Q-factor changes drastically. It is clear that as long as $|E| > \Delta_{\max}$ ($\Delta_{\max} = \Delta_0 Q^{(A)}_{\max}$), the averaged DOS repeats the linear part of the energy dependence of Eq. (13). In turn, at $|E| \lesssim \Delta_{\max}$, the averaged DOS is given by

$$\langle N_{2\mathrm{D}}(E)\rangle \approx \frac{a^2\Delta_{\max}}{2\pi\,\mathrm{A}^2}\left[1 - \frac{1}{2}\mathrm{erf}\left(\frac{U_1 - U_0}{\sqrt{2}W}\right) + \frac{1}{2}\mathrm{erf}\left(\frac{U_2 - U_0}{\sqrt{2}W}\right)\right], \tag{14}$$

where the functions $U_{1,2}(E)$ are the solutions of the quadratic equation $\Delta(U) = \Delta_0 Q^{(A)}(U) = E$, $U_1 > U_2$; also, the quantity U_0 is suggested to be well inside the interval (U_-, U_+); $\mathrm{erf}(\alpha)$ is the Gauss error function. Under the stipulation that $\widetilde{c} \ll 1$, the Q factor attains the maximum $Q^{(A)}_{\max} = 2\sqrt{\lambda\widetilde{c}}$ at $\widetilde{U} = \widetilde{U}_{\max} = \sqrt{\lambda}$, then the solutions of the equation $\Delta(U) = E$ take the simple form $\widetilde{U}_{1,2} = \sqrt{\lambda} \pm \sqrt{1 - \frac{\widetilde{E}}{2\sqrt{\lambda\widetilde{c}}}}$, $\widetilde{E} = \frac{E}{\Delta_0}$. This simplification yields the more apparent expression for the DOS:

$$\langle N_{2\mathrm{D}}(E)\rangle \approx \frac{a^2\Delta_{\max}}{2\pi\,\mathrm{A}^2}\left(1 - \frac{\sqrt{2}}{\sqrt{\pi}\widetilde{W}}\sqrt{1 - \frac{\widetilde{E}}{2\sqrt{\lambda\widetilde{c}}}}\right), \tag{15}$$

if the mean strength U_0 is close to $U_{\max}$, i.e., $|U_0 - U_{\max}| \ll W$, or

$$\langle N_{2\mathrm{D}}(E)\rangle \approx \frac{a^2\Delta_{\max}}{2\pi\,\mathrm{A}^2} \times \left[1 - \frac{1}{\sqrt{2\pi}\widetilde{W}}\exp\left(-\left(\frac{\sqrt{\lambda} - \widetilde{U}_0}{\sqrt{2}\widetilde{W}}\right)^2\right)\sqrt{1 - \frac{\widetilde{E}}{2\sqrt{\lambda\widetilde{c}}}}\right], \tag{16}$$

in the opposite case.

Given that the mean strength U_0 is close to one of two the critical values U_- or U_+, where the Q factor behaves as $\Delta_0 Q^{(A)} = \alpha_\pm(U - U_\pm)$, $\alpha_\pm = \Delta_0\frac{dQ^{(A)}}{dU}|_{U=U_\pm}$, $\alpha_- > 0$, $\alpha_+ < 0$, one obtains

$$\langle N_{2\mathrm{D}}(E)\rangle \approx \frac{a^2|E|}{4\pi\,\mathrm{A}^2}\left[\mathrm{erf}\left(\frac{U_- - U_0 + \frac{|E|}{\alpha_-}}{\sqrt{2}W}\right) - \mathrm{erf}\left(\frac{U_- - U_0 - \frac{|E|}{\alpha_-}}{\sqrt{2}W}\right)\right], \tag{17}$$

which is valid at $|E| \ll \Delta_0|Q^{(A)}_\infty|$. Hence, DOS falls to zero as E^2 near a surface Dirac point. Indeed, if the mean strength U_0 is close to $U_\pm$, i.e. $|U_0 - U_\pm| \ll W$, Eq. (17) reduces to

$$\langle N_{2\mathrm{D}}(E)\rangle \approx \frac{a^2E^2}{\sqrt{2\pi^3}|\alpha_\pm|W\,\mathrm{A}^2}. \tag{18}$$

In the opposite case, when $|U_0 - U_\pm| \gg W$, one arrives at

$$\langle N_{2\mathrm{D}}(E)\rangle \approx \frac{a^2E^2}{2\sqrt{2\pi^3}|\alpha_\pm|W\,\mathrm{A}^2}\exp\left[-\left(\frac{U_\pm - U_0}{\sqrt{2}W}\right)^2\right]. \tag{19}$$

Provided above is the rough estimation of possible behavior of the disorder-averaged DOS $\langle N_{2\mathrm{D}}(E)\rangle$, which specifically depends on the location of U within narrow window for some partial cases. However, the scheme outlined above is too simple to provide a full picture of the fermion states under the stipulation that ESP is no longer spatially uniform through out the sample surface.

V. INHOMOGENEOUS ESP APPROXIMATION: NEF DOMAIN WALLS AND BOUND STATES

Above we have established the coupling of NEF $\Delta^{(A,F)}(U) = \Delta_0 Q^{(A,F)}(U)$ with the ESP strength U, which

allows us assess the surface states gapping in an ideally uniform AFM TI sample. Now we turn to the question about the response of the topological surface state to an inhomogeneous electrostatic perturbation. The latter is associated with the antisite concentration fluctuations, and the ESP strength $U(x, y)$ is supposed to be rather smooth at the mean distance between the charged defects. Within our continual approach, the surface fermions experience NEF $\Delta^{(A,F)}(x, y)$ that is induced by the large-scale inhomogeneous ESP: $U(x, y) \to \Delta(x, y)$. It is notable that, in the AFM ground state, the gap function $\Delta^{(A)}(x, y)$ can change along the surface plane (x, y) both in magnitude and in sign. Further we focus on this case and omit the upper index, i.e., $\Delta^{(A)} = \Delta$. In depending on the ESP variation $U(x, y)$, the regions with positive, $\Delta(x, y) > 0$, and negative, $\Delta(x, y) < 0$, NEF exist at the surface. Between such regions, there appears a boundary of a peculiar type that we call NEF domain wall (DW).

Let us take a look at a particular one-dimensional (1D) ESP configuration, wherein the strength $U(x, y) = U(x)$ varies monotonically from $U(x \to -\infty) = U_L$ to $U(x \to \infty) = U_R$ passing through the critical value U_+ or U_-. Such a type of ESP creates NEF DW separating two insulating domains with opposite signs of the gap $\Delta(x \to -\infty) = \Delta_L$ and $\Delta(x \to \infty) = \Delta_R$, $\mathrm{sgn}(\Delta_R \Delta_L) < 0$, where values $U_{R,L}$ are mapped to ones $\Delta_{R,L}$ via Eqs. (7) and (11). The gap vanishes at the border line $x = x_0$, $\Delta(x_0) = 0$, where $U(x_0) = U_\pm$. It means that the surface Dirac fermion experiences a positive gapping on one side of the border, and a negative gapping on another side of the border. Since the fermion perceives NEF DW as a topological border between regions possessing distinct topological indices, a bound state is expected to occur at NEF DW.

To demonstrate that, taking into account the presence of a spatially dependent NEF term we rewrite the Hamiltonian Eq. (6) in a quasiclassical approximation as

$$H_{2D}(x, k_y) = \mathrm{A}\left(-i\sigma_y \frac{\partial}{\partial x} - k_y \sigma_x\right) + \Delta(x)\sigma_z. \tag{20}$$

Although the precise configuration of the inhomogeneous NEF is not known a priori, without loss of generality, we choose the spatial texture of a single DW in the following form:

$$\Delta(x) = \frac{\Delta_R + \Delta_L}{2} + \frac{\Delta_R - \Delta_L}{2} \tanh(\upsilon x), \tag{21}$$

where $\Delta_R > 0$ and $\Delta_L < 0$. The NEF within the upward and downward domain regions is rather uniform and changes gradually on the scale $\sim \upsilon^{-1}$ in the vicinity x_0. The NEF DW border runs along the $\boldsymbol{e}_y$ axis. The momentum k_y is a good quantum number playing the role of a parameter.

We effectively deal with a 1D quantum problem and look for the low-energy bound state $F^{(0)}(x, k_y)$ satisfying the equation $H_{2D}(x, k_y)F(x, k_y) = \omega(k_y)F(x, k_y)$ under the condition $F(|x| \to \infty, k_y) = 0$. This problem with the gap function Eq. (21) is exactly integrable. A straightforward calculation gives the EF spinor

$$F^{(0)}(x, k_y) = C\begin{pmatrix} 1 \\ -1 \end{pmatrix} \exp\left(-\frac{\Delta_R + \Delta_L}{2\mathrm{A}} x\right) \times [\cosh(\upsilon x)]^{-\frac{\Delta_R - \Delta_L}{2\mathrm{A}\upsilon}}, \tag{22}$$

where C is a normalized constant. The corresponding energy eigenvalue has a linear form $\omega_+^{(0)}(k_y) = \mathrm{A}k_y$, which crosses the exchange gaps related to both the right domain, $2\Delta_R$, and the left one, $2|\Delta_L|$. The fermion of Eq. (22) with a chirality $\sigma = +$ moves with velocity A along NEF DW, according to the spin-momentum locking rule. The EF Eq. (22) exponentially decays with distance from the wall as $\sim \exp(-\frac{\Delta_R}{\mathrm{A}} x)$ for $x > 0$ and $\sim \exp(-\frac{\Delta_L}{\mathrm{A}} x)$ for $x < 0$. One can easily write down EF for the state bound to NEF DW of opposite orientation, when $\Delta(x)$ changes sign from positive to negative with increasing coordinate x. In this case, one obtains a state with opposite chirality $\sigma = -$ and opposite velocity $\omega_-^{(0)}(k_y) = -\mathrm{A}k_y$.

In addition to the 1D gapless chiral state, NEF DW can carry 1D ordinary doubly degenerate states with a gapped spectrum $\omega^{(n)}(k_y) = \pm\sqrt{[\omega^{(n)}(0)]^2 + \mathrm{A}^2 k_y^2}$, $n = 1, 2, 3, \ldots$, which are similar to Volkov&Pankratov states [54]. These states emerge within the exchange gap, $|\omega^{(n)}(0)| < \min\{\Delta_R, |\Delta_L|\}$, when the gap function is sufficiently smooth at the EF spatial extension, i.e., $\upsilon^{-1} > \frac{2\mathrm{A}}{\Delta_R + |\Delta_L|}$. And their number is determined by the condition $n < N = \frac{|\Delta_R - \Delta_L|}{2\mathrm{A}\upsilon}\left(1 - \sqrt{\frac{|\Delta_R + \Delta_L|}{|\Delta_R - \Delta_L|}}\right)$. The explicit dependence of the nth energy level $\omega^{(n)}(0)$ on the model parameters $\Delta_{R,L}$, υ, and A is analyzed in Ref. [55]. At sharp NEF DW, when $\upsilon^{-1} < \frac{2\mathrm{A}}{\Delta_R + |\Delta_L|}$, only the topological chiral state with $n = 0$ appears. A smoother NEF DW hosts more bound states. In the limiting case $\upsilon^{-1} \gg \frac{2\mathrm{A}}{\Delta_R + |\Delta_L|}$ and, consequently, $N \to \infty$ the discrete spectral curves $\omega^{(n)}(k_y)$ tend to fill the whole exchange gap.

Thus, the energy spectrum of the surface AFM TI, containing a sufficiently smooth single NEF DW, is represented by not only the 1D chiral state with the linear dispersion $\omega^{(0)}(k_y) = \mathrm{A}k_y$ but also the 1D gapped branches $\omega^{(n)}(k_y)$ inside the exchange gap. Then, the contribution of all the 1D states to the in-gap DOS is given by

$$N_{1D}(E) = \frac{a}{2\pi\mathrm{A}} + \frac{a|E|}{\pi\mathrm{A}} \sum_{1 \leqslant n \leqslant N} \frac{h(E^2 - [\omega^{(n)}(0)]^2)}{\sqrt{E^2 - [\omega^{(n)}(0)]^2}}. \tag{23}$$

It should be emphasized that the topologically protected bound chiral state Eq. (22) is not much affected by the NEF DW shape as long as the constraint $\Delta(x \to \infty)\Delta(x \to -\infty) < 0$ is satisfied. In other words, this state is robust against local deformations of the gap function spatial profile $\Delta(x)$ in the context of supersymmetric quantum mechanics [56]. It demonstrates the linear dispersion relation $\omega_\pm^{(0)}(k_y) = \pm\mathrm{A}k_y$ and makes always a constant contribution $N_{1D}^{(0)}(E) = \frac{a}{2\pi\mathrm{A}}$ to DOS [the first term on the right-hand side of Eq. (23)], which only depends on the bulk spectrum parameter A. On the other hand, due to the dependence of the level $\omega^{(n)}(0)$ on the model parameters such as $\Delta_{R,L}$ and υ, the 1D gapped states $\omega^{(n)}(k_y)$ and their contribution to DOS [the last term on the right-hand side of Eq. (23)] are highly susceptible to the effect of local variation of the gap function $\Delta(x)$.

Given that the NEF domains have a finite spatial scale, one may find delicate features of the electron spectrum inherent to the multi-DW situation. Consider, for example, the

configuration of two parallel running NEF DWs of type of Eq. (22) and a domain region of the width l situated in between. The width l is defined as the distance between the positions where the gap function vanishes, while NEF is equal to $\Delta(x) = \Delta_S$ inside the domain region. Naturally, one suggests that $l \gg \{\frac{\mathrm{A}}{\Delta_S}; \frac{1}{\upsilon}\}$. The double-DW configuration hosts a pair of the 1D bound states of kind of $F^{(0)}$ (22) with opposite chiralities. An indirect coupling between these states with $n = 0$ appears due to virtual excitations through the 2D band/s $E(\boldsymbol{\kappa}) = \pm\sqrt{\mathrm{A}^2\kappa^2 + \Delta_S^2}$. As a result, the tiny minigap opens at the Γ point in the spectrum, $\omega_{\pm}^{(0)}(k_y) = \pm \mathrm{A}k_y \to \Omega_{\pm}^{(0)}(k_y) = \pm\sqrt{\eta^2 + \mathrm{A}^2k_y^2}$. The minigap size $2|\eta|$ can be shown to decay exponentially with increasing the inter-DW distance in such a way that $|\eta| \approx |\Delta_S| \exp(-\frac{|\Delta_S|}{\mathrm{A}} l)$ when $\upsilon^{-1} < \frac{\mathrm{A}}{|\Delta_S|}$. In the case of the smooth NEF DWs, the gap decaying may be evaluated as $|\eta| \sim \exp[-\frac{|\Delta_S|}{\mathrm{A}}(l - \frac{\varrho}{\upsilon})]$, where ϱ is within the interval $1 < \varrho < 2$. At the same time, the 1D gapped states with $n \geqslant 1$ are split in energy, $\omega^{(n)}(0) \to \omega^{(n)}(0) \pm \varsigma$, where ς is of the same order of magnitude as $|\eta|$.

Another issue specific to NEF DW is that the border $U(x, y) = U_{\pm}$ or $\Delta(x, y) = 0$, is not generally described with a straight line. Nevertheless, in the vicinity of the border with a big curvature radius R, one can introduce curvilinear coordinates, $(x, y) \to (\xi, \zeta)$, longitudinal ξ, and transversal ζ (normal to the border). Then, in a zero order in $\{\frac{1}{\upsilon R}, \frac{\mathrm{A}}{|\Delta_{R,L}|R}\} \ll 1$, one can the profile Eq. (21) as a gap function $\Delta(\zeta)$. Correspondingly, the low-energy bound states are approximated by 1D EFs $F^{(n)}(\zeta, k_\xi)$, localized about the border $\Delta(\zeta) = 0$, and the dispersion relations $\omega^{(n)}(k_\xi)$, k_ξ being a momentum associated with the coordinate ξ.

VI. SURFACE SPECTRAL PROPERTIES UNDER A STRONG ESP DISORDER

For a realistic AFM TI material, where disorder in spatial distribution of the antisite and other defects can play an essential role, the question arises of how a disorder affects the surface spectral properties. At large scale level, an electrostatic potential of the imperfect surface could be represented as a random mixture of different spatial regions extending $\sim L_i$, within which the ESP strength $U \approx U_i$ is rather uniform, i being the region's index. If these regions are sufficiently broad compared with the localization length, $L_i \gg \frac{\mathrm{A}}{|\Delta_i|}$, the surface band structure can roughly be presented as a superposition of the spectra $E_i(\boldsymbol{\kappa}) = \pm\sqrt{\mathrm{A}^2\kappa^2 + \Delta^2(U_i)}$ that stem from the domains with the corresponding net exchange energy $\Delta(U_i)$. The averaging over the ensemble of all realizations $\{U_i\}$ yields the surface spectrum with the exchange gap $\sim 2\sqrt{\langle\Delta^2(U_i)\rangle}$, the energy edges of which are smeared due to the potential disorder. The edge smearing may be estimated from Eqs. (14)–(16) and (17)–(19) for $\langle N_{2\mathrm{D}}(E)\rangle$, given that the strength U_i is implied to fluctuate within the narrow energy interval $\sim W_i$. Such a spectral picture is appropriate to the case of a weak disorder when the potential defects are pretty homogeneously distributed on the surface.

On a more detailed level, the electron topological state and magnetic texture on the surface of intrinsic AFM TI are intimately related, which can be manifested in strikingly various spectral behavior depending on a type of quenched disorder associated with random ESP $U(x, y)$. Under strong fluctuations of ESP, the NEF DWs come into play. As shown above, the boundary between regions with opposite NEF always harbors fermion state with the linear dispersion inside the gap. In a multi-domain situation, such boundaries get pinned at the zero-gap contours $\Delta(x, y) = 0$, along which the conditions $U(x, y) = U_+$ or $U(x, y) = U_-$ are satisfied. The NEF DW scale $\sim\upsilon^{-1}$ may significantly vary, formally, from zero (a sharp DW) to infinity (a extended DW). The averaging over a manifold of possible ESP configurations $\{U(x, y)\}$ entails that the surface restores spatial uniformity and azimuthal symmetry in the (x, y) plane on macroscopic scale significantly exceeding L_i. The averaged spectral density is expected to display a near perfect 2D conelike band, $\pm\Upsilon\kappa$, $\Upsilon \simeq \mathrm{A}$, at least near the Dirac point. Intuitively, such a low-energy gapless spectral image can be viewed as composed from the partial energy branches, $\omega^{(0)}(k_\xi) = \pm\mathrm{A}k_\xi$, of the 1D topologically robust states of kind of $F^{(0)}(x, k_\xi)$ Eq. (22) hosted by single NEF DWs running along different azimuthal directions. In this context, the 2D conelike band could be regarded as a topological protected one. The relation $\pm\Upsilon\kappa$ does not make sense of a dispersion law as a functional relation between excitation energy and momentum, since the latter is not a good quantum number and the corresponding state is not a steady one owing to absence of a long-range order at the surface. Moreover, the essential spectral feature like $\pm\Upsilon\kappa$ is found to be noticeable only at a sufficiently high density of NEF DWs.

In the multidomain situation, the surface in-gap DOS is only contributed by the low-energy gapless states $\omega^{(0)}(k_\xi) = \pm\mathrm{A}k_\xi$, induced by NEF DWs, when the latter occupy only a small fraction of the surface, i.e. $\upsilon^{-1} < \frac{2\mathrm{A}}{\Delta_R + |\Delta_L|}$. When the NEF DW texture is smoothed, the energetically lower-lying excitations with linear dispersion are complemented by the higher-lying ones stemmed from the gapped states $\omega^{(n)}(k_\xi)$, $n = 1, 2, 3, \ldots$, appearing under $\upsilon^{-1} > \frac{2\mathrm{A}}{\Delta_R + |\Delta_L|}$. The NEF fluctuations can cause a crucial broadening of the singularities in DOS at $|E| = \omega^{(n)}(0)$ in Eq. (23) (the second term on the right-hand side), because the band edges $\omega^{(n)}(k_\xi)$ are directly affected by the NEF DW texture details.

The 1D bound states originated from neighboring NEF DWs affect each other, which contributes to a gapping, $\sim 2|\eta|$, of the low-energy electron excitations near the Γ point. The coupling between these states is enhanced as NEF DWs get less spatially separated. When the characteristic lengths υ^{-1}, $\frac{\mathrm{A}}{|\Delta|}$ and l appear to be comparable to each other, the quasi-1D bound states overlap substantially, and the surface spectrum becomes structureless.

We have restricted the discussion to the case with $U_1 = -U_2$. By the way, when $U_1 \neq -U_2$, the surface bands are shifted in energy by $E_0(U_1, U_2)$ and the particle-hole symmetry is broken [25,51]. Hence, in the presence of disorder, the gap size in the surface spectrum is expected to be reduced effectively due to fluctuations of $E_0(U_1, U_2)$.

When an external magnetic field, applied normally to the surface, drives the interlayer magnetic coupling from AFM to FM, the band edges get clearer, the exchange gap increases up to value $2\Delta^{(F)}(\widetilde{U},\widetilde{c}) = 2\Delta_0 Q^{(F)}(\widetilde{U},\widetilde{c})$ and the in-gap states disappear along with NEF DWs.

VII. DISCUSSION AND CONCLUSION

The approach developed above to explain in a consistent manner the surface electron properties of intrinsic AFM TIs of the $MnBi_2Te_4$ like family is conceptually built on the five major ideas. First, we postulate that a regular magnetic order of the A-type with uniform magnetization in each SL and AFM coupling between neighboring SLs is persistent up to the surface of the material. This thesis has empirical support [37,42]. Second, the penetration depth of the topological state beneath the AFM TI (0001) surface is comparable with the long range magnetic order period. For that reason, the emergent NEF can be highly sensitive to potential perturbations. In the prototypical AFM TI $MnBi_2Te_4$, the perturbation is naturally caused by the native Mn_{Bi} and Bi_{Mn} antisite defects and the Te vacancies. Third, to design an impact of the charge defects upon the surface fermions, we incorporate ESP into the model calculations. Fourth, we argue analytically that the ESP strength drives NEF and, thereby, show how the electrostatic mechanism of the exchange gap modulation in the surface fermions dispersion works at a microscopic level. Fifth, it is found that NEF can change its sign as one varies the ESP strength. In such a case, NEF DWs on the surface plane engender 1D states with the linear dispersion that span the exchange gap.

We have conducted a proof-of-concept study of the above proposals and understood the genesis of the spectral features of the intrinsic AFM TI surface, which reflects profound interplay of the topological electronic states, magnetic order and electrostatic effects. On the one hand, the significant variation in the measured surface gap size from one sample to another [32] can be reasonably ascribed to the NEF evolution under the ESP strength. On the other hand, a gapless behavior of the surface states found in ARPES observations [34–39] can be closely tied to the 1D states originated from NEF DWs as long as strong electrostatic gradient exists along the surface. Our theoretical findings provide guidance to qualitatively clarify the origin of the spectroscopic peculiarities. The ARPES experimental data give a spectral image spatially averaged over the light spot of a micron scale. In our theory context, this image is formed mainly by the surface states which are hosted on the dominating NEF configurations $\Delta(x, y)$. For example, as ESP fluctuates slowly on a micron scale with a small deviation from a mean value U_0, the surface spectrum is expected to show the clear energy gap $\sim|2\Delta(U_0)|$ with the weak broadening of its edges. This is consistent with the observation in the ARPES measurements [12,28–31], where the good quality $MnBi_2Te_4$ samples were used. Otherwise, when the sample surface undergoes the strong disorder, so the ESP strength $|\widetilde{U}(x, y)|$ varies much over the lateral correlation length comparable or smaller than $\sim 10 - 100$ nm, the dense network of NEF DWs occurs at the surface. In this case, the spectrum exhibits a finite DOS inside the exchange gap with blurred energy edges. In fact, the gapless spectral features were observed in high-resolution ARPES measurements [34–39]. We propose that the observed conelike dispersion could be due to strong disorder of the cation intermixing in the $MnBi_2Te_4$ specimens under studies. Furthermore, when the ESP strength varies in a wide range, but the correlation length is more than $\sim$100 nm, the density of NEF DWs is too low to give any appreciable in-gap DOS. In such a situation, the domain regions with large positive NEF and small negative NEF contribute to the spectrum that displays a two-gap structure. Such an unusual feature in the ARPES image was witnessed by the authors of Ref. [33]. So, considering several different potential landscapes, we disentangle the possible spectroscopic regimes, which can be treated in terms of the NEF DWs density. Applying the external perpendicular magnetic field sufficient to align the moments in parallel, one can see solely the gapped spectrum with the enlarged gap, which size is not much dependent on the ESP strength and spatial disorder.

Thus, we unveil the underlying scenario behind shaping the surface electron structure in AFM TIs, which is based on the key role of the surface electrostatic effects. It is natural to associate these effects with the native antisite defects and other imperfections, the concentration and spatial distribution of which depend upon the fabrication conditions. Thereby, the proposed scenario not only reconciles the apparent disagreement between the rigid AFM order and the gapless spectrum but also successfully resolves the contradictions between the spectroscopic data on $MnBi_2Te_4$ obtained by different experimental groups.

The crystal structure of natural vdW superlattice $MnBi_4Te_7$ contains the magnetic SLs of $MnBi_2Te_4$ alternating with the nonmagnetic QLs of Bi_2Te_3. A number of ARPES studies of compound $MnBi_4Te_7$ [17,41,47,57–59] have identified the topological surface states on the two terminations: a gap state on the QL termination and a gapless Dirac-cone state on the SL termination. One can explain this behavior by suggesting that the QL and SL differ from each other in type and concentration of intrinsic point defects. Within our approach, it means that the QL termination and the SL termination have distinct ESPs. The $MnBi_4Te_7$ surface, most likely, is subjected to greater electrostatic modification on the SL termination than on the QL one. Hence, the exchange gap on the SL (magnetic) termination can be either significantly reduced due to the strong ESP, which shifts the gravity center of the surface state into the QL beneath or spanned due to the 1D states living at NEF DWs. At the same time, the exchange gap on the QL (nonmagnetic) termination can acquire finite size owing to a penetration of the surface state EF tail into the SL beneath. We expect that the presented concept can be readily extended to all family $MnBi_2Te_4(Bi_2Te_3)_n$.

We expect that the presented concept can be readily extended to the superlatticelike magnetic TIs $MnBi_2Te_4(Bi_2Te_3)_n$. In these systems, with increasing the inserted Bi_2Te_3 spacer thickness, the interlayer superexchange coupling is reduced significantly or switches from an AFM type to a FM one [60,61]. To estimate the surface exchange gap in the compounds $MnBi_2Te_4(Bi_2Te_3)_n$, one can apply Eqs. (11) and (12) for Q factors $Q^{(A)}(U, c)$ and $Q^{(F)}(U, c)$, in which c is the superlattice period.

The unique feature of the AFM TIs found within our minimal theoretical model is the presence of NEF DWs produced by the SP gradient. It should be emphasized that the origin of NEF DWs is essentially different from that of magnetic DWs, which either appear in the usual manner due to imperfections in bulk magnetic materials or come from atomic steps on rough surface of AFM material. Such magnetic DWs were found in $MnBi_2Te_4$ [42] and, as theoretically predicted in Refs. [62,63], they can also host 1D bound states. However, the distance between the neighboring magnetic DWs at the surface of $MnBi_2Te_4$ is of the order of $1-10\ \mu$m [42], which excludes the manifestation of the corresponding bound states in spectroscopy.

The strengths U_1 and U_2 encode the ESP felt by surface electrons characterized by the orbitals $|Pn+\sigma\rangle$ and $|Ch-\sigma\rangle$, respectively. In general case, near the $\bar{\Gamma}$ point, the surface spectrum can be written in the form $E(\boldsymbol{\kappa}) = E_0 \pm \sqrt{A^2\kappa^2+\Delta^2}$. Given that the Hamiltonian (1) is particle-hole symmetric, the energy shift of the surface bands $E_0(U_1,U_2)$ appears under the condition $U_1+U_2\neq 0$, for example, in the weak ESP case one has $E_0 = \frac{2q_0 d}{1+\lambda}(U_1+U_2)$. [25,51] In turn, the gap size is mainly determined by the difference U_1-U_2, i.e., by the difference of the contributions stemming from the orbitals $|Pn+\sigma\rangle$ and $|Ch-\sigma\rangle$, which has been demonstrated by Eqs. (5)–(8) and (11) and (12). In this sense, the ESP matrix elements match up the antisite and other defects presented in subsurface layers of the material. Without loss of the generality of the results, we restrict ourselves to the case of $U_1 = -U_2 = U$, when particle-hole symmetry keeping significantly facilitates the calculations.

To evaluate the ESP strength U, we can use the DFT calculation [32] which shows that the gap drops from ∼80 meV to almost zero when the surface potential gradient $\frac{dU}{dz}$ is changed from 0.3 $\frac{\text{eV}}{\text{Å}}$ to -0.5 $\frac{\text{eV}}{\text{Å}}$.

The authors of Ref. [64] proposed a scenario for the surface state gapping in the self-doped n-type $MnBi_2Te_4$, which is distinct from the above mentioned mechanisms [32,33,44]. They suppose that the gain from the electron energy lowering caused by the exchange gap closing can overcome the energy cost of the magnetic order deformation of DW type between the out-of-plane alignment in the bulk to the in-plane alignment at the surface. However, first, this assumption is not supported by the experimental observation of the robust AFM order up to the surface [42]. Second, in known ARPES measurements, there have not been any signs of the in-plane magnetization at the upmost SLs of $MnBi_2Te_4$ samples such as the Dirac cone shifting from the $\bar{\Gamma}$ point. In our theory, the magnetization reconfiguration near the surface of AFM TI could be treated as the NEF modulation induced by the ESP without resorting to idea of the AFM order deformation. To study the doping effects on the delicate interplay between magnetism and topology in intrinsic AFM TIs, within the analytical approach, the EF spatial distribution $\Theta(\mathbf{r})$ and the exchange gap 2Δ must be calculated in self-consistent manner under the given electron concentration. Furthermore, besides the superexchange interaction between magnetic moments, one needs to take into account the RKKY coupling mediated by free carriers.

In summary, we proposed the analytical approach for the underlying microscopic scenario behind the complex behavior of topological surface states of AFM TIs observed by photoelectron spectroscopy in $MnBi_2Te_4$. We specifically stress the key role played by the electrostatic surface potential which determines the value and sign of the exchange energy of the surface fermions. Within the model framework, we discuss the possible mechanisms driving the exchange gap size as well as origin of the in-gap states. The obtained results deepen our understanding of an interplay of band topology and magnetic ordering.

ACKNOWLEDGMENTS

We thank M. M. Otrokov for valuable discussions. E.V.C. acknowledges support from Saint Petersburg State University (Project ID No. 90383050). I.A.S. and V.N.M. acknowledge support from Russian Science Foundation within Research Project No. 18-12-00169-p.

[1] Y. Tokura, K. Yasuda, and A. Tsukazaki, Nat. Rev. Phys. **1**, 126 (2019).
[2] C.-Z. Chang, J. Zhang, X. Feng, J. Shen, Z. Zhang, M. Guo, K. Li, Y. Ou, P. Wei, L.-L. Wang *et al.*, Science **340**, 167 (2013).
[3] A. Sekine and K. Nomura, J. Appl. Phys. **129**, 141101 (2021).
[4] Y. Zhao and Q. Liu, Appl. Phys. Lett. **119**, 060502 (2021).
[5] D. M. Nenno, C. A. Garcia, J. Gooth, C. Felser, and P. Narang, Nat. Rev. Phys. **2**, 682 (2020).
[6] M. Mogi, M. Kawamura, R. Yoshimi, A. Tsukazaki, Y. Kozuka, N. Shirakawa, K. Takahashi, M. Kawasaki, and Y. Tokura, Nat. Mater. **16**, 516 (2017).
[7] M. Mogi, M. Kawamura, A. Tsukazaki, R. Yoshimi, K. S. Takahashi, M. Kawasaki, and Y. Tokura, Sci. Adv. **3**, eaao1669 (2017).
[8] D. Xiao, J. Jiang, J.-H. Shin, W. Wang, F. Wang, Y.-F. Zhao, C. Liu, W. Wu, M. H. Chan, N. Samarth *et al.*, Phys. Rev. Lett. **120**, 056801 (2018).
[9] S. Bhattacharyya, G. Akhgar, M. Gebert, J. Karel, M. T. Edmonds, and M. S. Fuhrer, Adv. Mater. **33**, 2007795 (2021).
[10] M. M. Otrokov, T. V. Menshchikova, M. G. Vergniory, I. P. Rusinov, A. Y. Vyazovskaya, Y. M. Koroteev, G. Bihlmayer, A. Ernst, P. M. Echenique, and A. Arnau, 2D Mater. **4**, 025082 (2017).
[11] R. S. K. Mong, A. M. Essin, and J. E. Moore, Phys. Rev. B **81**, 245209 (2010).
[12] M. M. Otrokov, I. I. Klimovskikh, H. Bentmann, D. Estyunin, A. Zeugner, Z. S. Aliev, S. Gaß, A. Wolter, A. V. Koroleva, A. M. Shikin *et al.*, Nature (London) **576**, 416 (2019).

[13] M. M. Otrokov, I. P. Rusinov, M. Blanco-Rey, M. Hoffmann, A. Y. Vyazovskaya, S. V. Eremeev, A. Ernst, P. M. Echenique, A. Arnau, and E. V. Chulkov, Phys. Rev. Lett. **122**, 107202 (2019).

[14] Y. Deng, Y. Yu, M. Z. Shi, Z. Guo, Z. Xu, J. Wang, X. H. Chen, and Y. Zhang, Science **367**, 895 (2020).

[15] C. Liu, Y. Wang, H. Li, Y. Wu, Y. Li, J. Li, K. He, Y. Xu, J. Zhang, and Y. Wang, Nat. Mater. **19**, 522 (2020).

[16] E. D. Rienks, S. Wimmer, J. Sánchez-Barriga, O. Caha, P. S. Mandal, J. Růžička, A. Ney, H. Steiner, V. V. Volobuev, H. Groiß *et al.*, Nature (London) **576**, 423 (2019).

[17] I. I. Klimovskikh, M. M. Otrokov, D. Estyunin, S. V. Eremeev, S. O. Filnov, A. Koroleva, E. Shevchenko, V. Voroshnin, A. G. Rybkin, I. P. Rusinov, M. Blanco-Rey, M. Hoffmann *et al.*, npj Quantum Mater. **5**, 54 (2020).

[18] J. Ge, Y. Liu, J. Li, H. Li, T. Luo, Y. Wu, Y. Xu, and J. Wang, Natl. Sci. Rev. **7**, 1280 (2020).

[19] K. He and Q.-K. Xue, SPIN **09**, 1940016 (2019).

[20] P. Wang, J. Ge, J. Li, Y. Liu, Y. Xu, and J. Wang, Innovation **2**, 100098 (2021).

[21] C.-Z. Chang and M. Li, J. Phys.: Condens. Matter **28**, 123002 (2016).

[22] X. Kou, Y. Fan, M. Lang, P. Upadhyaya, and K. L. Wang, Solid State Commun. **215-216**, 34 (2015).

[23] V. N. Men'shov, I. A. Shvets, and E. V. Chulkov, JETP Lett. **110**, 771 (2019).

[24] V. N. Men'shov, I. A. Shvets, V. V. Tugushev, and E. V. Chulkov, Phys. Rev. B **96**, 075302 (2017).

[25] V. N. Men'shov, I. A. Shvets, and E. V. Chulkov, Phys. Rev. B **99**, 115301 (2019).

[26] J. Li, Y. Li, S. Du, Z. Wang, B.-L. Gu, S.-C. Zhang, K. He, W. Duan, and Y. Xu, Sci. Adv. **5**, eaaw5685 (2019).

[27] D. Zhang, M. Shi, T. Zhu, D. Xing, H. Zhang, and J. Wang, Phys. Rev. Lett. **122**, 206401 (2019).

[28] R. Vidal, H. Bentmann, T. Peixoto, A. Zeugner, S. Moser, C.-H. Min, S. Schatz, K. Kißner, M. Ünzelmann, C. Fornari *et al.*, Phys. Rev. B **100**, 121104(R) (2019).

[29] S. H. Lee, Y. Zhu, Y. Wang, L. Miao, T. Pillsbury, H. Yi, S. Kempinger, J. Hu, C. A. Heikes, P. Quarterman *et al.*, Phys. Rev. Res. **1**, 012011(R) (2019).

[30] A. Zeugner, F. Nietschke, A. U. Wolter, S. Gaß, R. C. Vidal, T. R. Peixoto, D. Pohl, C. Damm, A. Lubk, R. Hentrich *et al.*, Chem. Mater. **31**, 2795 (2019).

[31] D. A. Estyunin, I. I. Klimovskikh, A. M. Shikin, E. F. Schwier, M. M. Otrokov, A. Kimura, S. Kumar, S. O. Filnov, Z. S. Aliev, M. B. Babanly *et al.*, APL Mater. **8**, 021105 (2020).

[32] A. M. Shikin, D. A. Estyunin, N. L. Zaitsev, D. Glazkova, I. I. Klimovskikh, S. O. Filnov, A. G. Rybkin, E. F. Schwier, S. Kumar, A. Kimura *et al.*, Phys. Rev. B **104**, 115168 (2021).

[33] A. M. Shikin, D. A. Estyunin, I. I. Klimovskikh, S. O. Filnov, E. F. Schwier, S. Kumar, K. Miyamoto, T. Okuda, A. Kimura, K. Kuroda *et al.*, Sci. Rep. **10**, 13226 (2020).

[34] Y.-J. Hao, P. Liu, Y. Feng, X.-M. Ma, E. F. Schwier, M. Arita, S. Kumar, C. Hu, M. Zeng, Y. Wang *et al.*, Phys. Rev. X **9**, 041038 (2019).

[35] H. Li, S.-Y. Gao, S.-F. Duan, Y.-F. Xu, K.-J. Zhu, S.-J. Tian, J.-C. Gao, W.-H. Fan, Z.-C. Rao, J.-R. Huang *et al.*, Phys. Rev. X **9**, 041039 (2019).

[36] Y. Chen, L. Xu, J. Li, Y. Li, H. Wang, C. Zhang, H. Li, Y. Wu, A. Liang, C. Chen *et al.*, Phys. Rev. X **9**, 041040 (2019).

[37] P. Swatek, Y. Wu, L.-L. Wang, K. Lee, B. Schrunk, J. Yan, and A. Kaminski, Phys. Rev. B **101**, 161109(R) (2020).

[38] D. Nevola, H. X. Li, J.-Q. Yan, R. G. Moore, H.-N. Lee, H. Miao, and P. D. Johnson, Phys. Rev. Lett. **125**, 117205 (2020).

[39] C. Yan, S. Fernandez-Mulligan, R. Mei, S. H. Lee, N. Protic, R. Fukumori, B. Yan, C. Liu, Z. Mao, and S. Yang, Phys. Rev. B **104**, L041102 (2021).

[40] B. Chen, F. Fei, D. Zhang, B. Zhang, W. Liu, S. Zhang, P. Wang, B. Wei, Y. Zhang, Z. Zuo *et al.*, Nat. Commun. **10**, 4469 (2019).

[41] Y. Hu, L. Xu, M. Shi, A. Luo, S. Peng, Z. Wang, J. Ying, T. Wu, Z. Liu, C. Zhang *et al.*, Phys. Rev. B **101**, 161113(R) (2020).

[42] P. M. Sass, J. Kim, D. Vanderbilt, J. Yan, and W. Wu, Phys. Rev. Lett. **125**, 037201 (2020).

[43] Y. Yuan, X. Wang, H. Li, J. Li, Y. Ji, Z. Hao, Y. Wu, K. He, Y. Wang, Y. Xu *et al.*, Nano Lett. **20**, 3271 (2020).

[44] M. Garnica, M. M. Otrokov, P. C. Aguilar, I. I. Klimovskikh, D. Estyunin, Z. S. Aliev, I. R. Amiraslanov, N. A. Abdullayev, V. N. Zverev, M. B. Babanly *et al.*, npj Quantum Mater. **7**, 7 (2022).

[45] J.-Q. Yan, Q. Zhang, T. Heitmann, Z. Huang, K. Y. Chen, J.-G. Cheng, W. Wu, D. Vaknin, B. C. Sales, and R. J. McQueeney, Phys. Rev. Mater. **3**, 064202 (2019).

[46] M. Liu, C. Lei, H. Kim, Y. Li, L. Frammolino, J. Yan, A. H. Macdonald, and C.-K. Shih, PNAS **119**, e2207681119 (2022).

[47] X. Wu, J. Li, X.-M. Ma, Y. Zhang, Y. Liu, C.-S. Zhou, J. Shao, Q. Wang, Y.-J. Hao, Y. Feng *et al.*, Phys. Rev. X **10**, 031013 (2020).

[48] M.-H. Du, J. Yan, V. R. Cooper, and M. Eisenbach, Adv. Funct. Mater. **31**, 2006516 (2021).

[49] F. Hou, Q. Yao, C.-S. Zhou, X.-M. Ma, M. Han, Y.-J. Hao, X. Wu, Y. Zhang, H. Sun, C. Liu *et al.*, ACS Nano **14**, 11262 (2020).

[50] A. Tan, V. Labracherie, N. Kunchur, A. U. B. Wolter, J. Cornejo, J. Dufouleur, B. Büchner, A. Isaeva, and R. Giraud, Phys. Rev. Lett. **124**, 197201 (2020).

[51] V. N. Men'shov, V. V. Tugushev, T. V. Menshchikova, S. V. Eremeev, P. M. Echenique, and E. V. Chulkov, J. Phys.: Condens. Matter **26**, 485003 (2014).

[52] V. N. Men'shov, V. V. Tugushev, and E. V. Chulkov, JETP Lett. **97**, 258 (2013).

[53] V. N. Men'shov, V. V. Tugushev, and E. V. Chulkov, JETP Lett. **104**, 453 (2016).

[54] B. A. Volkov and O. A. Pankratov, Sov. J. Exp. Theor. Phys. Lett. **42**, 178 (1985).

[55] S. Tchoumakov, V. Jouffrey, A. Inhofer, E. Bocquillon, B. Plaçais, D. Carpentier, and M. Goerbig, Phys. Rev. B **96**, 201302(R) (2017).

[56] F. Cooper, A. Khare, and U. Sukhatme, Phys. Rep. **251**, 267 (1995).

[57] C. Hu, K. N. Gordon, P. Liu, J. Liu, X. Zhou, P. Hao, D. Narayan, E. Emmanouilidou, H. Sun, Y. Liu *et al.*, Nat. Commun. **11**, 97 (2020).

[58] K. N. Gordon, H. Sun, C. Hu, A. G. Linn, H. Li, Y. Liu, P. Liu, S. Mackey, Q. Liu, N. Ni *et al.*, arXiv:1910.13943.

[59] N. H. Jo, L.-L. Wang, R.-J. Slager, J. Yan, Y. Wu, K. Lee, B. Schrunk, A. Vishwanath, and A. Kaminski, Phys. Rev. B **102**, 045130 (2020).

[60] H. Sun, B. Xia, Z. Chen, Y. Zhang, P. Liu, Q. Yao, H. Tang, Y. Zhao, H. Xu, and Q. Liu, Phys. Rev. Lett. **123**, 096401 (2019).

[61] H. Deng, Z. Chen, A. Wolos, M. Konczykowski, K. Sobczak, J. Sitnicka, I. V. Fedorchenko, J. Borysiuk, T. Heider, L. Plucinski, K. Park *et al.*, Nat. Phys. **17**, 36 (2021).

[62] V. N. Men'shov, I. P. Rusinov, and E. V. Chulkov, JETP Lett. **114**, 699 (2021).

[63] I. P. Rusinov, V. N. Men'shov, and E. V. Chulkov, Phys. Rev. B **104**, 035411 (2021).

[64] W. Chen, Y. Zhao, Q. Yao, J. Zhang, and Q. Liu, Phys. Rev. B **103**, L201102 (2021).